.

TRIBHUVAN UNIVERSITY

INSTITUTE OF ENGINEERING

PULCHOWK CAMPUS

THESIS NO: M-20-MSMDE-2018/2020

Theoretical Performance Analysis of Fixed Pitch Propeller Operating at Low Reynolds Number Condition

by

Milan Adhikari

A THESIS

SUBMITTED TO THE DEPARTMENT OF MECHANICAL AND AEROSPACE ENGINEERING

IN PARTIAL FULFILLMENT OF THE REQUIREMENTS FOR THE DEGREE OF MASTER OF SCIENCE IN MECHANICAL SYSTEMS DESIGN AND ENGINEERING

DEPARTMENT OF MECHANICAL AND AEROSPACE ENGINEERING

LALITPUR, NEPAL

JULY, 2020

COPYRIGHT

TRIBHUVAN UNIVERSITY

INSTITUTE OF ENGINEERING

PULCHOWK CAMPUS

DEPARTMENT OF MECHANICAL ENGINEERING

The undersigned certify that they have read, and recommended to the Institute of Engineering for acceptance, a thesis entitled “Theoretical Performance Analysis of Fixed Pitch Propeller Operating at Low Reynolds Number Condition" submitted by Milan Adhikari in partial fulfillment of the requirements for the Degree of Master of Science in Mechanical Systems Design and Engineering.

Supervisor, Laxman Poudel, Ph.D.

Professor

Department of Mechanical and Aerospace Engineering

Supervisor, Hari Bahadur Dura

Assistant Professor

Department of Mechanical and Aerospace Engineering

External Examiner, Hari Prasad Neopane, Ph.D.

Professor

Department of Mechanical Engineering, Kathmandu University

Committe Chairperson, Nawaraj Bhattrai, Ph.D.

Head of Department

Department of Mechanical and Aerospace Engineering

Date:

ABSTRACT

The propeller performance data at its design point and off design points are the basis for the selection of suitable propeller for an unmanned air vehicles (UAVs) system. Various research have been conducted for the development of a tool for theoretical prediction of the propeller performance but are not readily available in the public domain. In addition, the commercially available propellers only have performances at design point. Thus, the current work focuses on developing an analytical tool for the prediction of the propeller performance which is based on the Blade Element Momentum Theory (BEMT). An arbitrary base line propeller has been designed for developing the current tool. The airfoil properties at various radial sections have been calculated from the XFOIL and the tool has been developed in Matrix Laboratory (MATLAB). The output from the developed tool was compared with existing experimental data for Harrington rotor 1 and thin electric APC 11x8 propeller. The preliminary calculations were carried out at the rotating speed and free stream velocity of 7500 RPM and 80 m/s respectively. The capability of the prediction tool were then explored at various operating conditions. The rotating speed and forward speed were changed from 6500 RPM to 8500 RPM and from 65 m/s to 90 m/s respectively. The performance analysis was done for the base line propeller to study the effects of rotational speed, free-stream velocity and advanced ratio. For the base line propeller at its design point, the thrust coefficient, torque coefficient and propulsive efficiency were calculated to be 0.0724, 0.0347 and 83.5% respectively. One way fluid structure interaction analysis was performed in ANSYS to study blade stress due to pressure and centrifugal loading. The comparison of BEMT prediction with CFD result was performed for baseline propeller at design point.

ACKNOWLEDGEMENTS

I would like to express my sincere gratitude to Prof. Dr. Laxman Poudel and Asst. Prof. Hari Bahadur Dura for supervising my thesis work. Without their continuous support and guidance, this research work would not have completed in time.

I am thankful to the Department of Mechanical and Aerospace Engineering for providing access to computational resources.

I am extremely greatful to Er. Lokesh Silwal, a graduate student in Department of Aerospace Engineering, Auburn University, USA for his continuous help and motivation throughout this thesis work.

I would like to thank my beloved family; my mother Mrs. Jandavi Adhikari, my father Mr. Trilochan Adhikari and brother Mijash Adhikari for the continuous support and motivation. I would not be here today without them.

I would like to thank my firends Er. Sudin Bhuju Shrestha, Er. Hemanta Dualal, Er. Anil Sapkota, Er. Rojesh Shrikhakar, Er. Sandip Thakur, Er. Prabesh Raj Devkota, Er. Nipesh Regmi, Er. Shailendra Rana and Er. Shishir K Das for their help and support during research work.

Lastly, I would like to thank all of the professors, lecturers and my colleagues from Department of Mechanical Engineering, Pulchowk Campus for their encouragement and support in completion of this thesis work.

TABLE OF CONTENTS

LIST OF FIGURES

LIST OF TABLES

LIST OF SYMBOLS

η	Propulsive Efficiency
λ	Rotor Inflow Ratio
λ_c	Climb Inflow Ratio
λ_i	Induced Inflow Ratio
ω	Rotational Speed
ϕ	Inflow Angle
ρ	Air Density
σ	Blade Solidity
θ	Blade Angle
a	Lift Curve Slope
a_0	Axial Velocity Correction Factor
a_1	Radial Velocity Correction Factor
B	Number of Blade
c	Chord Length
C_D	Drag Coefficient
C_L	Lift Coefficient
C_P	Power Coefficient
C_Q	Torque Coefficient
C_T	Thrust Coefficient
D	Diameter of Propeller
J	Advanced Ratio

P	Power
Q	Torque
R	Radius of Blade
r	Normalized Radial Position
Re	Reynolds Number
T	Thrust
V_∞	Free-stream Velocity
v	Induced Velocity

LIST OF ABBREVIATIONS

UAV	Unmanned Air Vehicles
BEMT	Blade Element Momentum Theory
RPM	Revolution Per Minute
MATLAB	Matrix Laboratory
CFD	Computational Fluid Dynamics
FSI	Fluid Structure Interaction
ANSYS	Analysis System

CHAPTER ONE: INTRODUCTION

1.1 Background

Application of UAVs is increasing in various fields such as search and rescue operation, agricultural, atmospheric research, surveying and medical delivery worldwide. The number of research pertaining to the design, performance and navigation of the drones has increased drastically over the recent years. In the context of Nepal, there is a recent surge in the interest in UAVs and drones with applications extending from civil to military sectors. But the amount of research carried out in Nepal in this field has been limited. One of the recent studies carried out in Nepal focused on developing baseline guidance for navigation and control system for medical delivery UAVs (Bhattarai et al., 2018). There is a need for the increased number of similar research in the field of drones with applications specific to the topology of Nepalese terrains. Thus, this thesis work is aimed at making a small contribution to the growing field of UAVs and drones by developing a low-fidelity tool that can easily be adapted by the end-user to make vital operating decisions.

1.2 Problem Statement

The availability of the propeller performance data at the design point and off-design points helps the designer to select the appropriate propeller for a specific application. The performance data that are easily available and cataloged systematically are mostly for the larger propeller with diameter 4 feet and more, which operates at high Reynolds number (Merchant & Miller, 2006). Because of the smaller chord length, the operating Reynolds number is low for the propeller which is used in small UAVs. There is not sufficient performance data for propeller operates in low Reynolds number (Brandt & Selig, 2011). Various researches have been conducted to develop a tool for the prediction of propeller performance using BEMT but are not available in the public domain (Park et al., 2018; McCrink & Gregory, 2017). The performance of the propeller varies according to its operating conditions because of the resultant Reynolds number and air density. But the manufacturer of commercially available propeller provides the propeller performance at its design point only which is not sufficient for the selection of propeller

for specific operating conditions. Thus, the main motive of this thesis work is to develop a low fidelity propeller performance prediction tool based on BEMT using the MATLAB programming language.

1.3 Objectives

1.3.1 Main Objective

The main objective of this thesis work is to develop a propeller performance prediction tool based on the combined blade element momentum theory.

1.3.2 Specific Objectives

The main objective of the research will be met by obtaining the following specific objectives.

i. To develop a propeller performance prediction tool by implementing combined BEMT in MATLAB programming language.

ii. To validate the developed tool using propeller data from existing literature.

iii. To analyze the performance of the baseline propeller at its design and off-design point using the developed tool.

iv. To perform one way fluid structure interaction analysis of the designed baseline propeller.

v. To compare the output of BEMT prediction with CFD analysis result for baseline propeller at design and off-design points.

1.4 Scope and Limitation

Most of the commercially available propeller for small UAVs are designed with two blades and fixed pitch. So the study is limited to the performance analysis of the fixed pitch propeller with two blades. The aerodynamics data for airfoil was generated using XFOIL. Previous research shows that the output of XFOIL shows good agreement with experimental and CFD analysis within stall regions (Günel et al., 2016; Traub & Cooper, 2008). This research is limited to the study of propeller performance within an

operational bound which will constrain the angle of attack of the sectional airfoil within the stall range.

CHAPTER TWO: LITERATURE REVIEW

2.1 Airfoil Basics

The cross-section of a propeller is an airfoil. Airfoils produce lifting force by creating the aerodynamic pressure difference between its upper and lower surface which are also called the suction and pressure surface of an airfoil. Figure 2.1 shows the basic terminologies of an airfoil. The leading and trailing edge mark the front and back of an airfoil and also separate the upper and lower surfaces. The chord line joins the leading edge and trailing edge with a straight line. If the upper and lower surfaces are the mirror images of each other about the chord line the air foil is called a symmetric. Mean camber line is the line constructed by joining the points between the upper and lower surfaces. The maximum distance between the mean camber line and chord line is called the camber of the airfoil section (Wall, 2012).

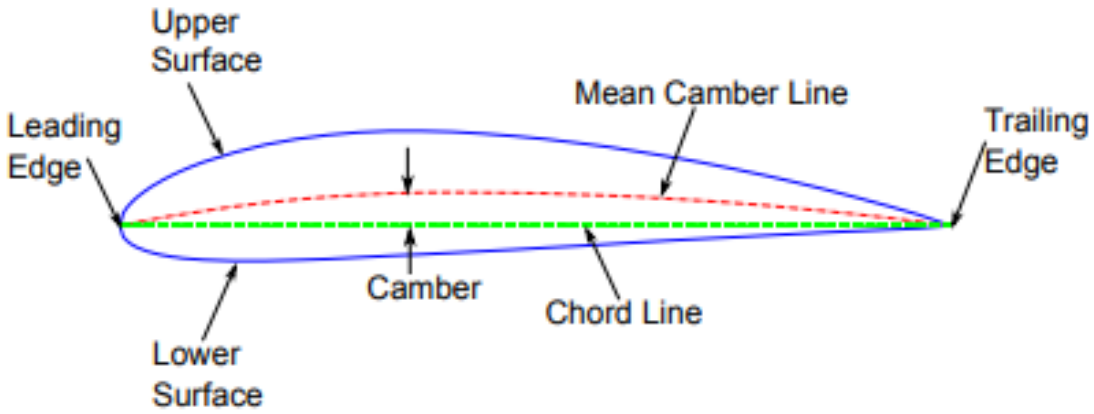

Figure 2.1: Basic Airfoil Nomenclature (Wall, 2012)

2.2 Propeller Basics

The propellers are rotating wings that produce lift in the direction of the rotational axis by creating pressure difference between forward and rare surfaces. Figure-2.2 shows the velocity diagram for the cross-section of a propeller. Any cross-section along the blade of the propeller is an airfoil with its specific characteristics.

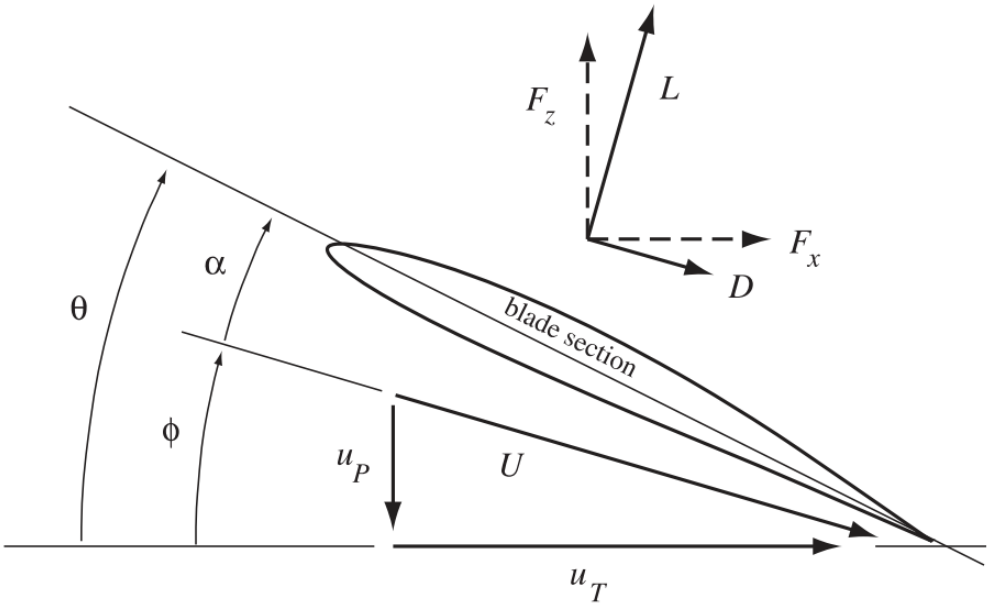

Figure 2.2: Blade Cross-section Velocity Triangle (Wall, 2012)

The blade of the propeller is connected to the engine shaft through the hub. The blade angle beta is the resultant angle between free stream velocity and the rotational velocity components. The pitch of the propeller is defined by the forward distance travel by the propeller in one rotation.

2.2.1 Geometry

Propellers are very similar to the wings. Blades are the lifting surface of a propeller. Most of the propellers have two to four blades. Any arbitrary cross-section of a blade has all the characteristics as an airfoil which is defined by its leading and trailing edge, mean camber line, chord line, thickness, etc. The blade is connected to the engine shaft through the hub and the area between the hub and the blade is called the root. The area of the blade opposite to the hub is called its tip. A propeller geometry with its various parts is shown in figure-2.3.

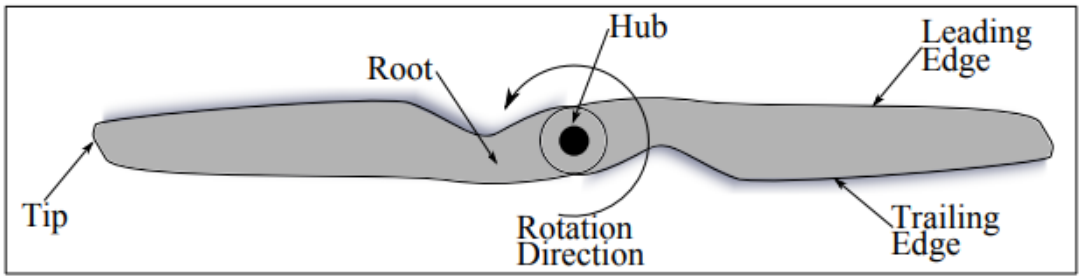

Figure 2.3: Propeller Geometry (Wall, 2012)

2.2.2 Propeller Performance Matrices

The performance of a propeller is measured using various indicators such as thrust coefficient, torque coefficient, power coefficient, and propulsive efficiency. Values of these performance indicators depend upon the geometrical parameters as well as operating conditions. In this section, various non-dimensional parameters that are used to describe the performance of a propeller are presented.

i. Advanced Ratio

The advanced ratio is a non-dimensional parameter, which quantifies the effects of forward motion and rotational speed on the performance of a propeller. Mathematical expression for the advanced ratio is,

$$J = \frac{V_\infty}{nD} \tag{2.1}$$

ii. Thrust, Torque and Power Coefficients

Thrust, torque, and power coefficients of a propeller are non-dimensional quantities relating to the thrust, torque, and power-producing capacity of a propeller to its rotational speed and diameter. The mathematical expression for thrust coefficient, torque coefficient and power coefficient from the dimensional analysis are shown below respectively,

$$C_T = \frac{T}{\rho n^2 D^4} \tag{2.2}$$

$$C_Q = \frac{Q}{\rho n^2 D^5} \tag{2.3}$$

$$C_P = \frac{P}{\rho n^3 D^5} \tag{2.4}$$

iii. Propulsive Efficiency

Propulsive efficiency is the ratio between powers transferred to the air by moving propeller to the mechanical power required to drive the propeller. Mathematically propulsive efficiency can be expressed as

$$\eta_{propulsive} = \frac{TV_\infty}{2\pi nQ} = \frac{C_T J}{2\pi C_Q} \tag{2.5}$$

Propulsive efficiency is used to compare the propeller with different geometric configuration or operational conditions.

2.3 Propeller Theories

Momentum theory, blade element theory, combined blade element momentum theory, and vortex or strip analysis theory are the analytical model used for propeller performance analysis. Combined BEMT was used by various researchers on their research for design and performance prediction of propeller used in small UAVs (McCrink & Gregory, 2017; Park et al., 2018). The corrected model of BEMT to incorporate the tip loss factor, Mach number correction, and three-dimensional flow correction was used by (McCrink & Gregory, 2017). Combined BEMT is being used for the design of the propeller because of its low computational cost. Here the explanation and equation of momentum theory, blade element theory, and combined blade element momentum theory were taken from Johnson (2013).

2.3.1 Momentum Theory

Momentum theory uses the laws of mass, momentum, and energy conservation to the rotor and flow as a whole and estimates the rotor performance. It relates the overall flow velocities to the total rotor thrust and power. In momentum theory, the rotor is modeled as an actuator disk. An actuator disk is a circular surface having zero thickness which can support a pressure difference but no velocity difference and thus accelerate the air through the disk. Actual rotor is approximated by the actuator disk model. The infinite number of rotor blades are considered in the actuator disk model. Because of

this assumption, the detailed flow of actuator disk is different from that of a real rotor with the finite number of rotor blades.

2.3.2 Blade Element Theory

Blade element theory calculates the forces on the blade section, then integrates those values in the radial direction to get forces and performance of the entire rotor. Each section of the blade is considered as a two-dimensional airfoil which produces aerodynamic forces, with the influences of the wake and the rest of the rotor contained entirely in an induced angle of attack at the section. The solution thus requires an estimate of wake induced velocity at the rotor disk, which is provided by momentum theory. Blade element theory deals with the detailed flow and blade loading and hence is the foundation of most of propeller aerodynamics.

2.3.3 Combined Blade Element Momentum Theory

Blade element theory combines the basic principles from both blade element and momentum approaches. Blade element momentum analysis of the propeller discretizes the blade into the number of sections in the radial direction. Then each element is considered as a 2D lifting element as in Figure-2.2, with no relation to the neighboring element. The sectional circumferential and axial force can be found by applying force balance to the blade element in both circumferential and axial directions respectively.

According to Blade element theory, the differential thrust and the differential power on an annulus of the disk on all blades of width dr at radial station r as,

$$dC_T = \frac{\sigma a}{2}(\theta - \frac{\lambda}{r})r^2 dr \tag{2.6}$$

$$dC_P = [\frac{\sigma a}{2}(\theta r\lambda - \lambda^2) + \frac{\sigma c_d r^2}{2}]r dr \tag{2.7}$$

The differential form of momentum theory gives,

$$dT = 2\rho dA(V_\infty + v)v \tag{2.8}$$

$$dC_T = 4\lambda\lambda_i r\, dr \tag{2.9}$$

Where $\lambda_i = v/\Omega R$ is the induced inflow ratio, $\lambda_c = V_\infty/\Omega R$ is the climb inflow ratio and $\lambda = \lambda_c + \lambda_i$. By using the differential form of momentum theory, the induced velocity at radial station r is assumed to be due to the thrust dT at that station. By equating the expression of dCT from blade element and momentum theory gives

$$\lambda^2 + (\frac{\sigma a}{8} - \lambda_c)\lambda - \frac{\sigma a}{8}\theta r = 0 \tag{2.10}$$

Which has the solution

$$\lambda = \sqrt{(\frac{\sigma a}{16} - \frac{\lambda_c}{2})^2 + \frac{\sigma a}{8}\theta r} - (\frac{\sigma a}{16} - \frac{\lambda c}{2}) \tag{2.11}$$

This equation gives the non-uniform inflow distribution. For given value of twist, pitch and chord, the inflow can be calculated as a function of r and λ_c, and then the rotor thrust and power can be calculated.

2.4 Airfoil Performance Database

The aerodynamic data of the airfoil that is being used in the propeller blade section is the main inputs for the BEMT model and the accuracy of those data determines the accuracy of prediction by the BEMT model. During the operation at design and off-design point, the propeller blade is operated in various Reynolds number and angle of attack. So the aerodynamic database which contains the lift and drags coefficient for the operating range of angle of attack and Reynolds number should be constructed.

There are different established codes for calculating two-dimensional lift and drag coefficient of an airfoil. XFOIL is an open source panel code developed by Drela (1989) which gives the coefficient of lift and coefficient of drag for a range of angle of attacks with varying Reynolds number. Morgado et al. (2016) compared the output of XFOIL with the conventional k–ω SST turbulence model and k -kl – transition closure model and found that the output of XFOIL is as good as the other used model. McCrink & Gregory (2017) used aerodynamic data obtained from XFOIL for their BEMT model to predict the performance of the different propeller.

CHAPTER THREE: RESEARCH METHODOLOGY

For the baseline propeller, the design parameters such as flight altitude, freestream velocity, and RPM were defined at its design point. A propeller geometry was selected by defining diameter, airfoil, the radial distribution of chord, and geometric angle. The operating condition was defined and the range of sectional Reynolds number and angle of attack was calculated. A three-dimensional database of airfoil aerodynamic properties was created in MATLAB using output from XFOIL. BEMT algorithm was implemented in MATLAB to develop a theoretical performance prediction tool. The validation of prediction tool was done by comparing output from tools with experimental data of Harrington Rotor1 (Harrington, 1951) and thin electric APC 11x8 propeller (Brandt & Selig, 2011). The performance parameters such as thrust coefficient, torque coefficient, and propulsive efficiency were predicted for the baseline propeller for the defined range of operating conditions. For baseline propeller comparison between CFD and BEMT results at the design point and off-design points was made. The flowchart for the methodology is presented in figure-3.1.

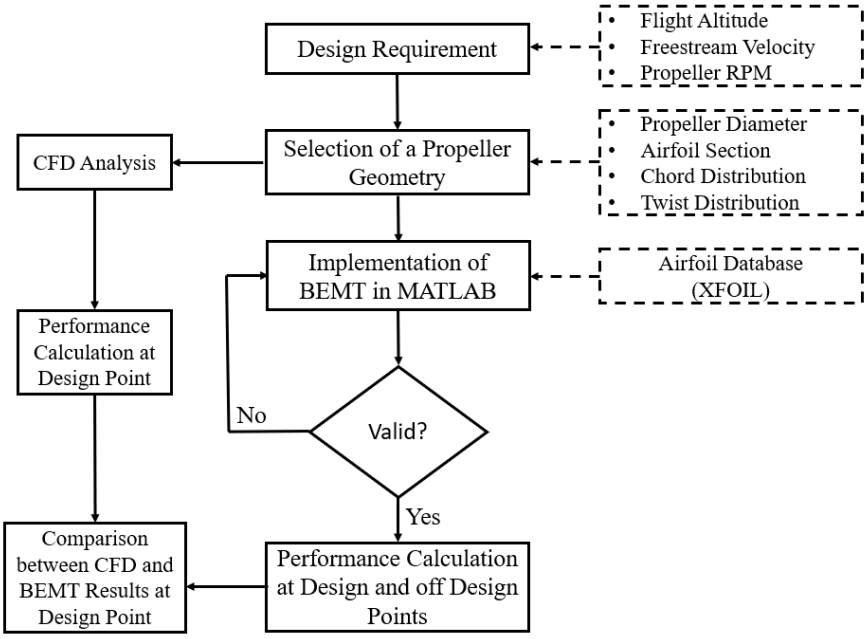

Figure 3.1: Research Methodology Flowchart

3.1 Design Requirements and Operating Conditions

The propeller is to be designed for high altitude applications. The operating elevation of the propeller was set to be 4000 m from sea level and the values of density and viscosity at this elevation were obtained from Sissenwine et al. (1962). For the design point, the rotational speed was set to 7500 RPM . The forward speed of the propeller at its design point was set to 80 m/s based on its application. Table-3.1 summarizes the operating condition of the designed propeller.

Table 3.1: Operating Conditions of Propeller

Parameters	Minimum	Maximum
Rotational Speed, RPM	6500	8500
Forward Speed, m/s	65 m/s	90 m/s

3.2 Propeller Geometry Selection

Based on design requirements a propeller geometry for the baseline propeller was designed. The design basis of various components with values is explained below.

3.2.1 Diameter Selection

The diameter of the propeller was taken as 10 inches i.e 0.254 m because most of the commercially available propellers which are being used in small UAVs have a diameter around this value.

3.2.2 Sectional Airfoil

For the simplicity a single airfoil section NACA 2412 was selected as the sectional airfoil throughout the propeller blade.

3.2.3 Radial Distribution of Chord Length

The chord distribution of the propeller airfoil section with respect to its radial position was calculated based on the relation below provide by Liu & He (2017).

$$\begin{aligned} c =&(0.084241 - 0.85789r + 4.7176r^2 - 9.6225r^3 \\ &+ 8.5000r^4 - 2.7959r^5)D \end{aligned} \tag{3.1}$$

Where c is the local chord length, r is the normalized radial position and D is the diameter. Figure-3.2 shows the radial distribution chord length of baseline propeller.

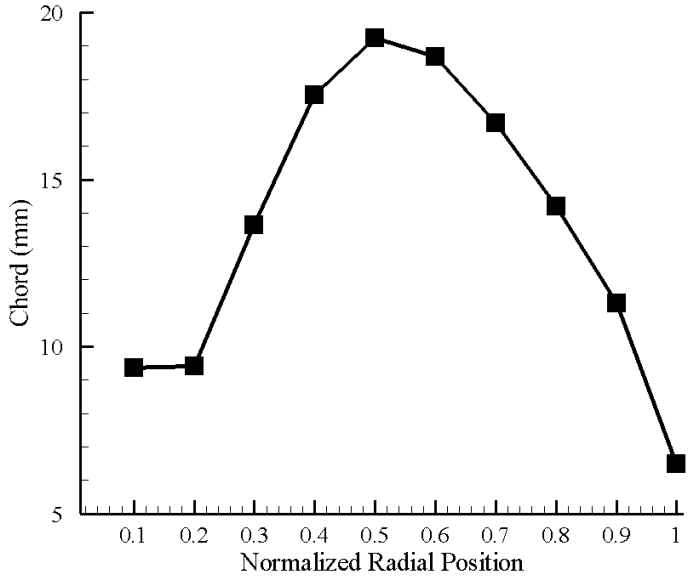

Figure 3.2: Radial Distribution of Chord Length

3.2.4 Radial Distribution of Blade Angle

Propeller operates with maximum efficiency if all the airfoil sections along the blade span are operating at their maximum efficient angle of attack. For the basic design of the propeller, the local Reynolds number for each section of the blade was set to be 50,000, which was the local Reynolds number value for the mid-span of the blade.

From the aerodynamics database, the most efficient angle of attack for selected airfoil at Reynolds number value 50,000 was found to be 5 degrees. Based on this, from the velocity triangle of each section the geometric angle for different normalized radial

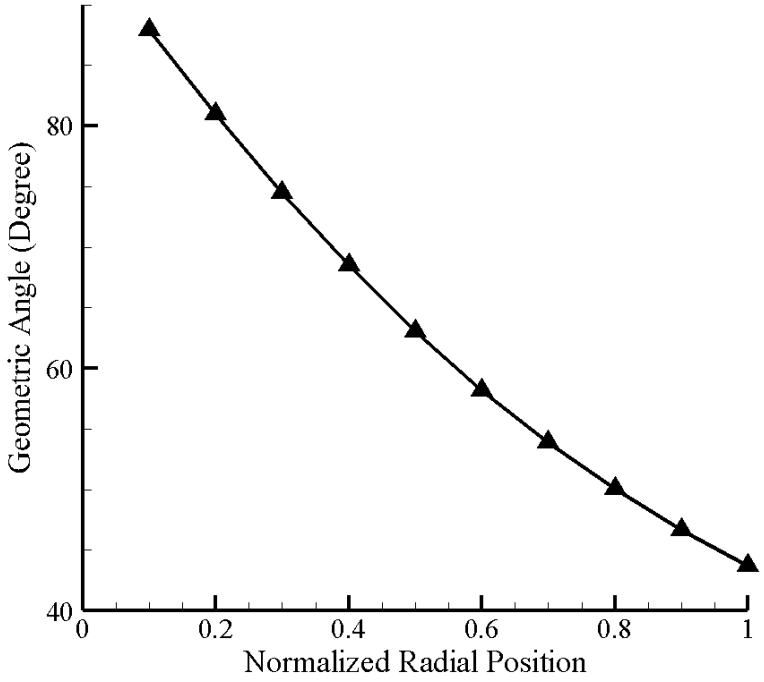

Figure 3.3: Radial Distribution of Geometric Angle

positions were calculated by adding the desired operating angle of attack i.e. 5 degrees with the local inflow angle calculated from the operating rotational and forward velocity at the design point. Figure 3.3 shows the obtained radial distribution of the geometric angle.

3.3 Airfoil Aerodynamic Database

For the designed propeller operated in its operational bound, it was found that the sectional Reynolds number varies from 20000 to 110000. An aerodynamic database that contains the variation of lift and drag coefficient with respect to angle of attack was created using XFOIL for the operating range of Reynolds number. A three-dimensional matrix was created with the angle of attack, lift, and drag coefficient and Reynolds number as the variables. Figure-3.4 and figure-3.5 show the representative aerofoil aerodynamic database for Re 20,000, 45,000, and 75,000 for the NACA 2412 airfoil section.

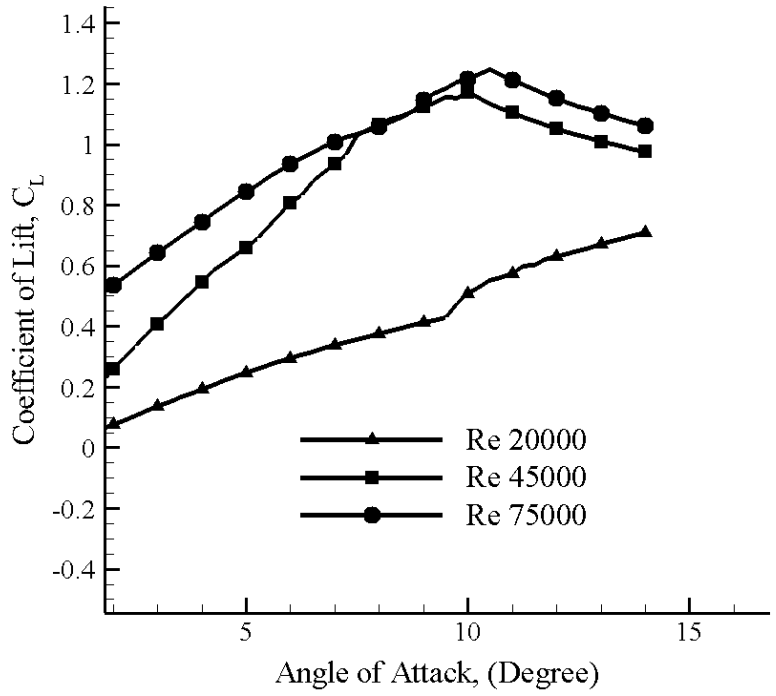

Figure 3.4: Angle of Attack vs Lift Coefficient

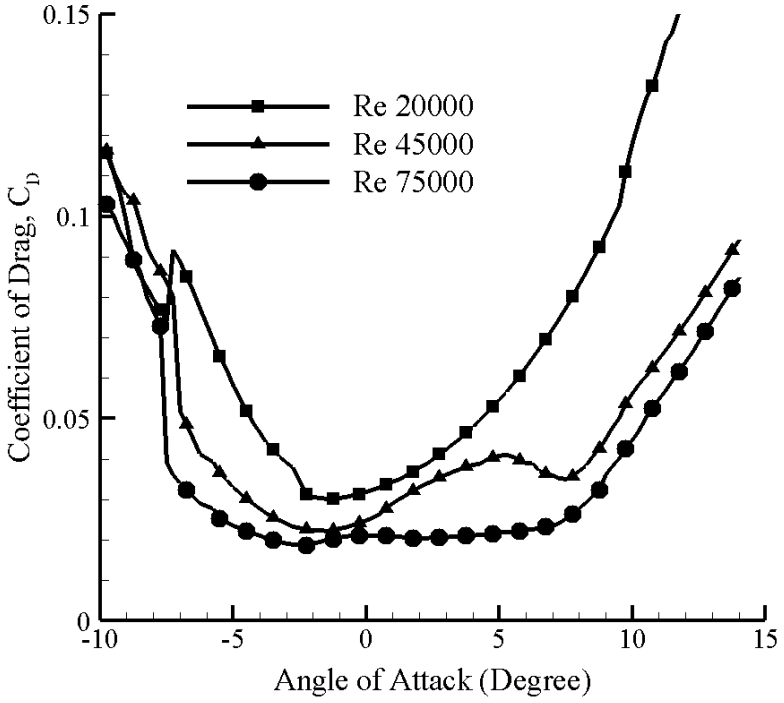

Figure 3.5: Angle of Attack vs Drag Coefficient

It was observed that the airfoil stalled at angles close to 10 degrees for larger Reynolds number of 45,000 and 75,000. For smaller Reynolds number of 20,000, the linear range for the airfoil was observed to be below 10 degrees. The plot for the drag coefficient (Figure 3.5) is also in part with the lift coefficient plot as a sudden increase in drag after the stall angle was observed.

3.4 BEMT Algorithm

The blade element momentum theory is the combination of momentum theory and blade element theory of propeller analysis. The momentum theory assumes the rotor plane to be a sheet with zero thickness which can sustain the pressure difference between the surfaces. The aerodynamic performances of the rotors are calculated based on the induced velocity imparted by the pressure difference. The momentum theory does not take into account the finite number of blades that the rotors have and thus can lead to large prediction errors. On the other hand, the blade element theory calculates the rotor properties on each radial section. The blade element momentum theory integrates the finite blade calculations of the blade element theory into the momentum theory to give a better prediction model. All the equations presented below were taken from McCrink & Gregory (2017). The differential thrust (dT) for each blade section as given by the blade element theory is shown below:

$$dT = \frac{1}{2}\rho V_\infty^2 cB\frac{(1+a_0)^2}{\sin^2\phi}C_T dr \tag{3.2}$$

Where B is the number of blades, a_0 is the axial inflow correction factor and ϕ is the local inflow angle. The differential torque for each blade section as given by the blade element theory is given by the equation below:

$$dQ = \frac{1}{2}\rho V_\infty cB\omega r^2\frac{(1+a_0)(1-a_1)}{\sin\phi\cos\phi}C_Q dr \tag{3.3}$$

Where r is radial position, ω is rotational velocity in rad/sec and a_1 is radial inflow correction factor. From equation 3.2 and 3.3, C_T and C_Q are related to the local lift and drag coefficients as,

$$\begin{bmatrix} C_T \\ C_Q \end{bmatrix} = \begin{bmatrix} \cos\phi & -\sin\phi \\ \sin\phi & \cos\phi \end{bmatrix} + \begin{bmatrix} C_L \\ C_D \end{bmatrix} \tag{3.4}$$

The conservation of momentum between the upstream and downstream of propeller gives the differential thrust as

$$dT = 4\pi r \rho V_\infty^2 (1 + a_0) a_0 dr \tag{3.5}$$

and the differential torque as

$$dQ = 4\pi r^3 \rho V_\infty (1 + a_0) a_1 dr \tag{3.6}$$

From equations 3.2, 3.3, 3.5 and 3.6 an implicit relationship for induced velocity components are obtained as follow:

$$a_0 = \frac{1}{(4\sin^2\phi/\sigma C_T) - 1} \tag{3.7}$$

$$a_1 = \frac{1}{(4\sin\phi\cos\phi/\sigma C_Q) + 1} \tag{3.8}$$

Where σ is the local solidity of the blade and is given by $cB/2\pi r$. Both radial and axial inflow correction factors are determined iteratively. Figure 3.6 illustrates the propeller performance prediction method using BEMT.

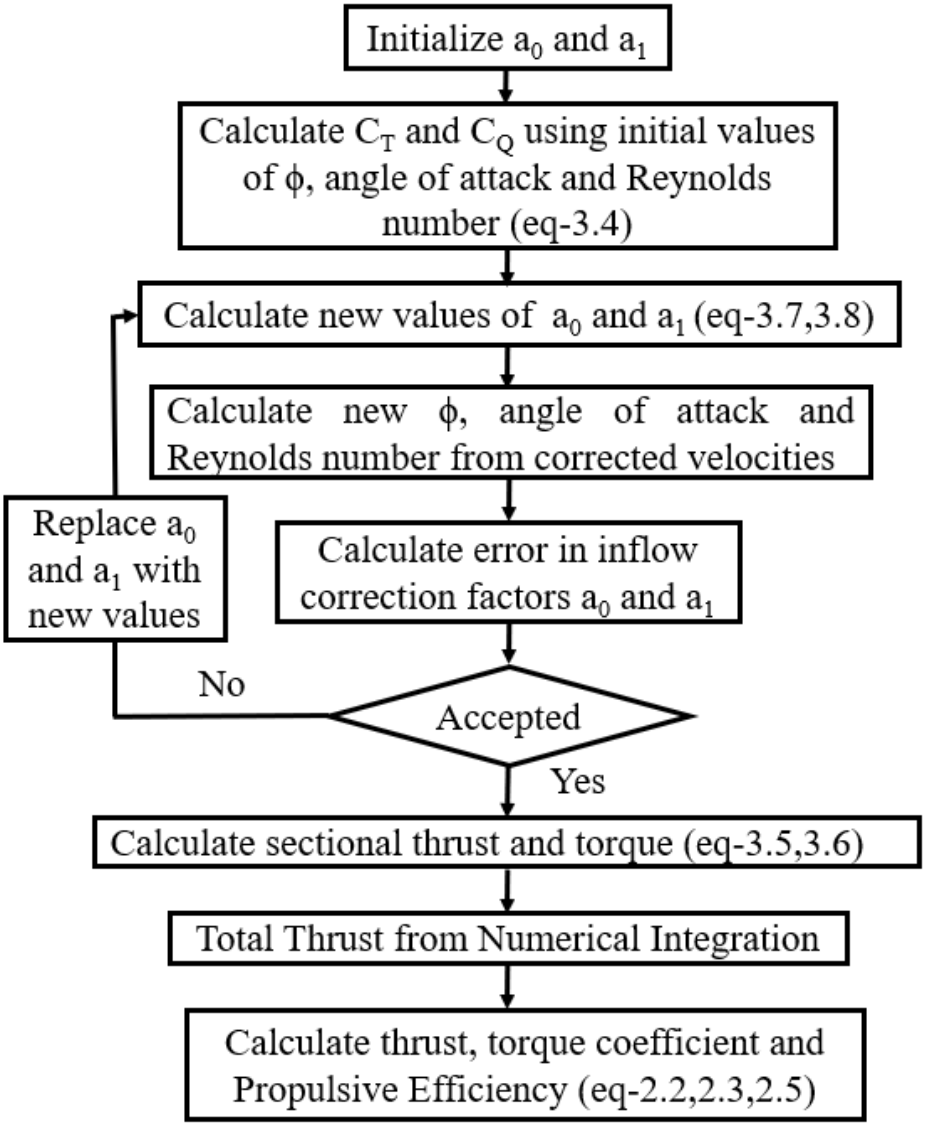

Figure 3.6: BEMT Algorithm Flowchart

3.5 Design Aspect

3.5.1 3d Modeling of Propeller

After setting the radial distribution of chord length and blade angle, scaling, transformation, and rotation actions for the NACA 2412 coordinates were performed to obtain the three-dimensional co-ordinates of the propeller section at the different radial position.

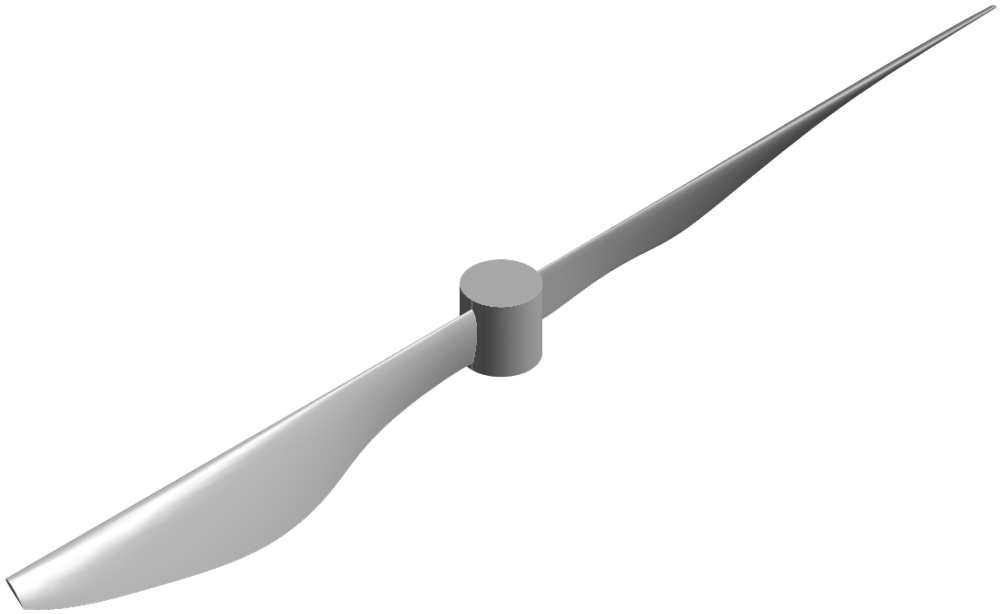

Figure 3.7: Isometric View of Baseline Propeller

The obtained coordinates were imported to SOLIDWORKS and by using the loft feature the blade profile was generated. For this purpose, a different MATLAB code was written which is presented in APPENDIX-C.

3.5.2 One Way FSI Analysis

CFD analysis was performed for the baseline propeller at the design point in ANSYS Fluent. The pressure load from the CFD analysis was imported to the structure and the total deformation, as well as the equivalent stress on the propeller blade were observed.

CHAPTER FOUR: RESULTS AND DISCUSSIONS

4.1 Validation of Prediction Tool

In this section, the validation of the BEMT algorithm and prediction tool was performed. For the validation of the BEMT algorithm, the output was compared with full-scale tunnel test data performed by Harrington (1951). The developed prediction tool was used to predict the performance of thin electric APC 11x8 propeller and the output was compared with experimental findings from Brandt & Selig (2011).

4.1.1 Harrington Rotor 1

The model of the classical BEMT currently developed was validated by comparing it with the full-scale experimental results. The full-scale data was extracted from a study carried out by Harrington (Harrington, 1951). Harrington rotor was a two-bladed rotor with a diameter of 7.62 m. The rotor solidity was 0.027. The rotors were operating at the tip speed of 152.4 m/s. The blade section used was untwisted with tapered plan form and thickness ratio. NACA four-digit symmetric airfoil section was used for the Harrington rotor. The comparison of the results from the current BEMT code with the results from the Harrington rotor is shown in Figure-4.1.

The plot shows the variation in the thrust coefficient with respect to the coefficient of power. From the figure, it was observed that there was a good agreement between the theoretical and experimental results. The plot shows a good fit until the thrust value of around 0.002. The deviation between the theoretical and experimental results above the thrust coefficient of 0.002 might be due to stall effects. The stalling phenomena in the experimental conditions are not predicted by the BEMT theory which could be one of the possible explanation for the deviation. The other reason might be due to the underlying assumption of the BEMT itself, i.e., the assumption of the small angle of attack. The small angle assumption is violated at higher thrust values which might be the other possible explanation for the observed deviation.

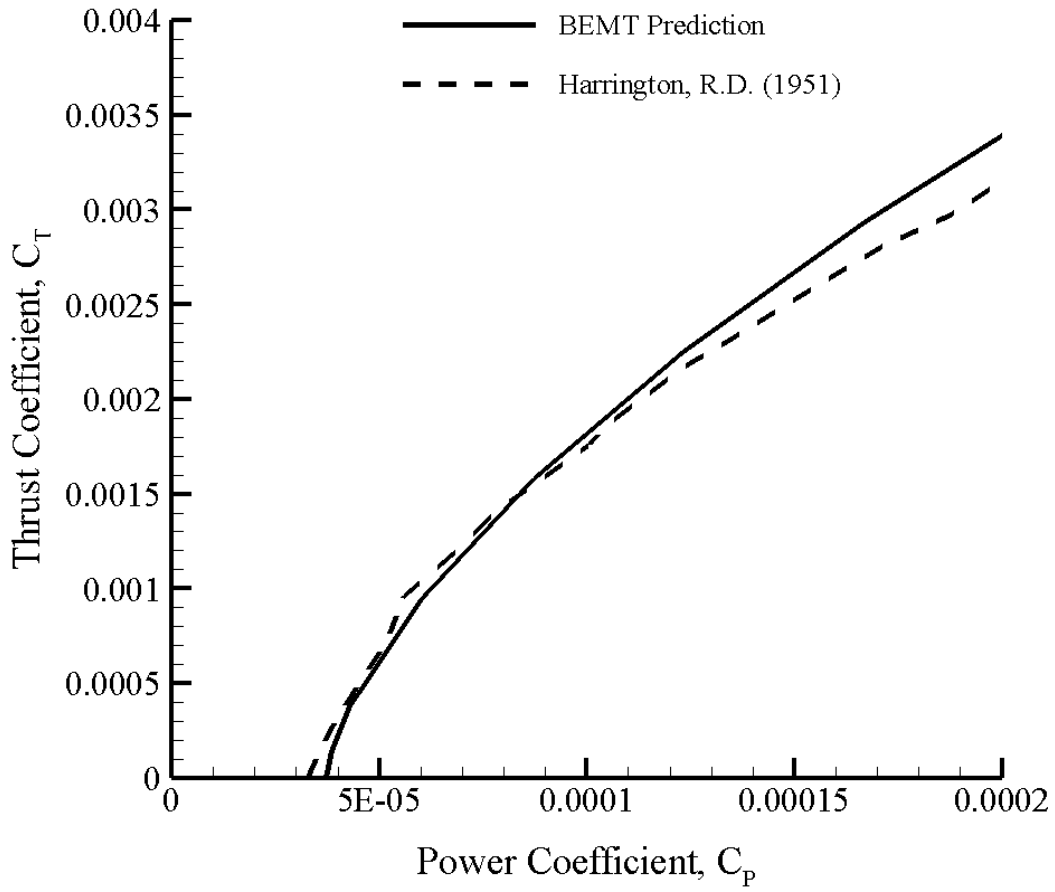

Figure 4.1: Comparison of Full Scale Tunnel Test Data and BEMT Prediction for Harrington Rotor 1

Besides the small angle assumption, inviscid flow and thin airfoil are other underlying assumptions in the classical BEMT. The inviscid assumption is valid for full-scale operations where the Reynolds numbers are in the order of millions. At high Reynolds number, the inertial effects are more dominant compared to the viscous effects. Thus, the classical BEMT is adequate for predicting the performance of the full-scale rotors. But for the low Reynolds number case, the classical BEMT fails to produce reliable results. Thus, modifications in the classical BEMT has been done to include the effects of large angles of attack and viscosity. The database from the XFOIL software has been used to include these effects and the results from the modified BEMT have been discussed in the next sections.

4.1.2 Thin Electric APC 11 x 8

Before using the developed prediction tool for the performance analysis of the baseline propeller its result needs to be validated against existing data. For this purpose, the experimental performance data of the thin electric APC 11x8 propeller was extracted from Brandt & Selig (2011). For the propeller geometry, the radial distribution of blade angle and chord length were also extracted from the same literature. APC propeller website mentioned that the thin electric propeller uses Eppler E63 airfoil for the blade section. The aerodynamic performance database was created for Eppler E63 airfoil using XFOIL for the range of Reynolds number from 10000 to 100000 within the stall range. The variation of thrust coefficient and propulsive efficiency were predicted using the developed tool and compared with experimental data.

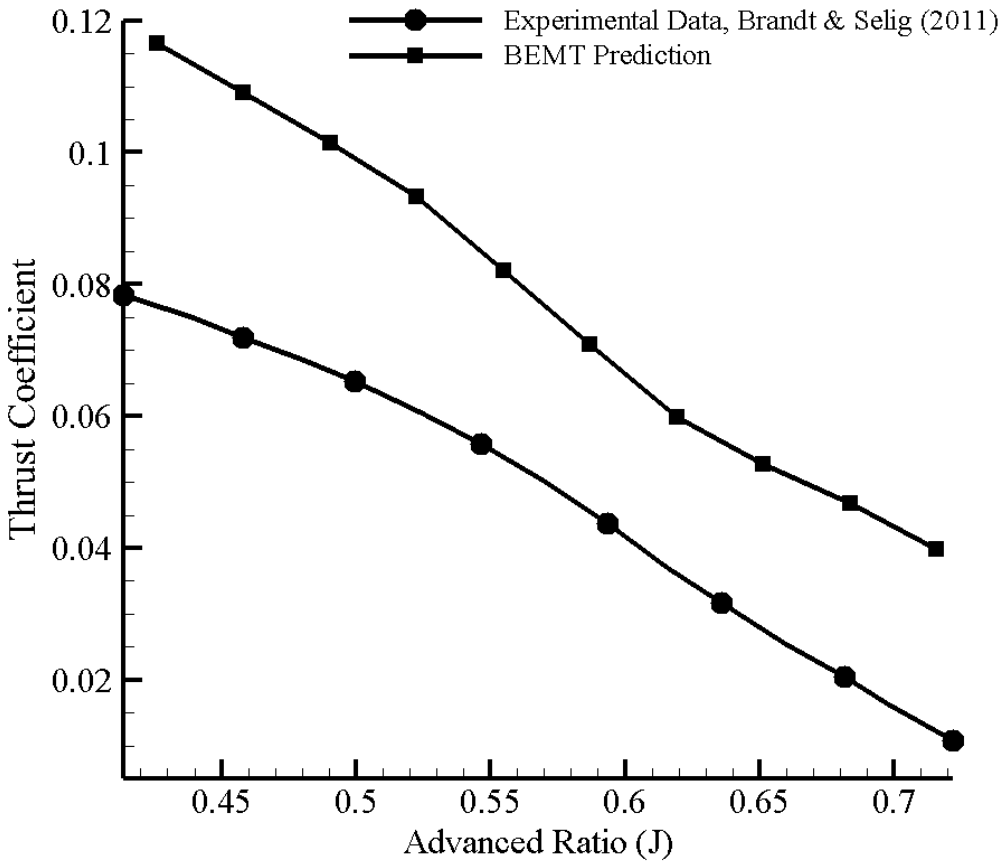

Figure 4.2: Comparison of Thrust Coefficient

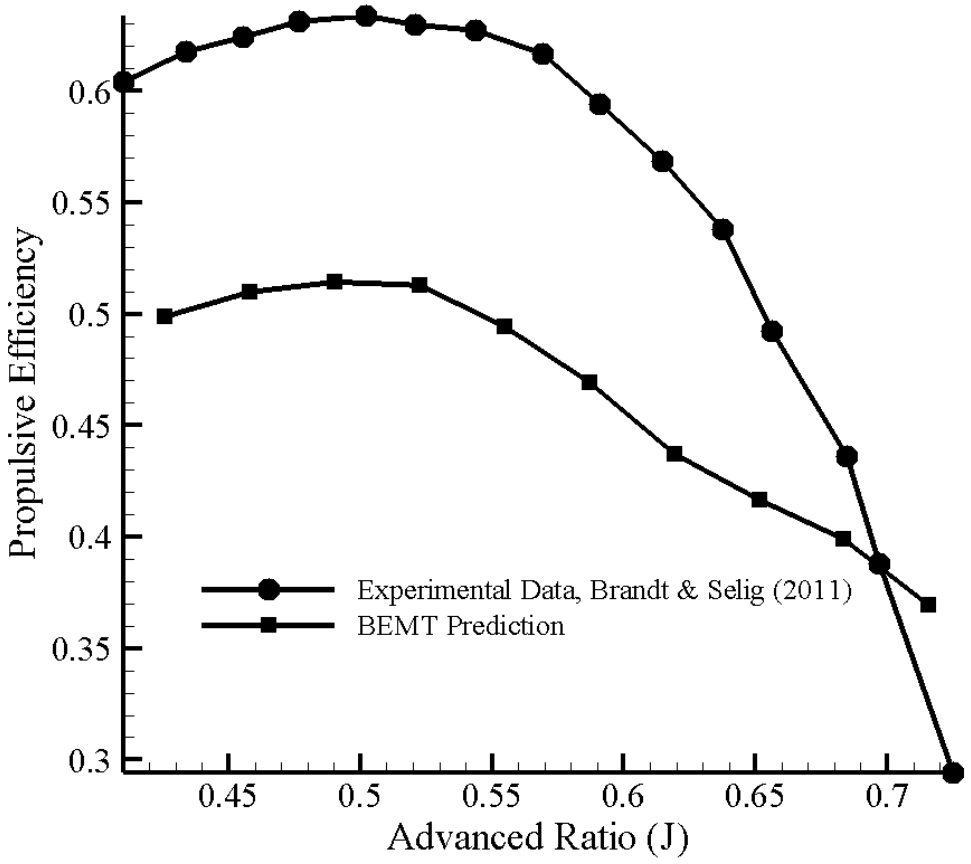

Figure 4.3: Comparison of Propulsive Efficiency

In figure-4.2 it can be seen that the predicted values of the thrust coefficient follow the same trend that of experimental data measured by Brandt & Selig (2011) but overestimated for all range of advanced ratio. A similar result was presented by MacNeill & Verstraete (2017) while comparing experimental findings with BEMT prediction. For the defined operational bound, the maximum variation in the thrust coefficient was found to be 51.83% when the advanced ratio is 0.42.

Similarly, the comparison of BEMT prediction and experimental data was made for variation in propulsive efficiency and shown in figure-4.3. For propulsive efficiency, it was observed that BEMT prediction underestimated its value for most of the advanced ratios. But when the advanced ratio is greater than 0.71 BEMT overestimated propulsive efficiency.

4.2 Effect of Rotational Speed

After validation of the BEMT model with existing experimental data, the results from the model were analyzed at different operating conditions. The rotational speed of the propeller was varied from 6700 RPM to 8500 RPM with freestream velocity varied as 70 m/s, 80 m/s, and 90 m/s. The variation of thrust coefficient, torque coefficient, and propulsive efficiency with respect to the rotational speed of the propeller has been discussed in this section.

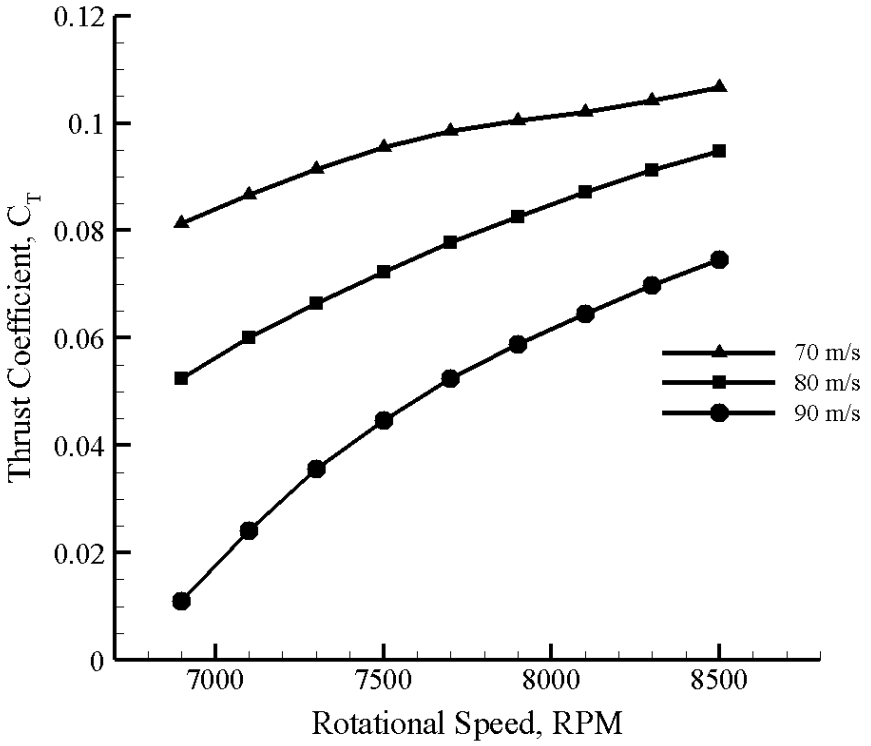

Figure 4.4: Variation of Thrust Coefficient with Rotational Speed

Figure-4.4 shows the variation of thrust coefficient with respect to rotational speed for different free stream velocities. From the figure, it can be seen that the thrust coefficient of the rotors increased with increasing rotational speed for a constant freestream velocity. The increased thrust is due to the increase in the tangential velocity component in the velocity triangle (u_T) as shown in figure-2.2. The increase in the u_T increases the effective angle of attack in the velocity triangle which consequently increases the thrust produced by the rotors. Following this argument, for the same rotational speed, the thrust should decrease with increasing the freestream velocity due to an increase in induced

velocity component (u_p). The increase in the induced velocity reduces the effective angle of attack and thus, reducing the thrust value. The current argument is confirmed by the figure where the minimum thrust is observed for the case of maximum freestream velocity.

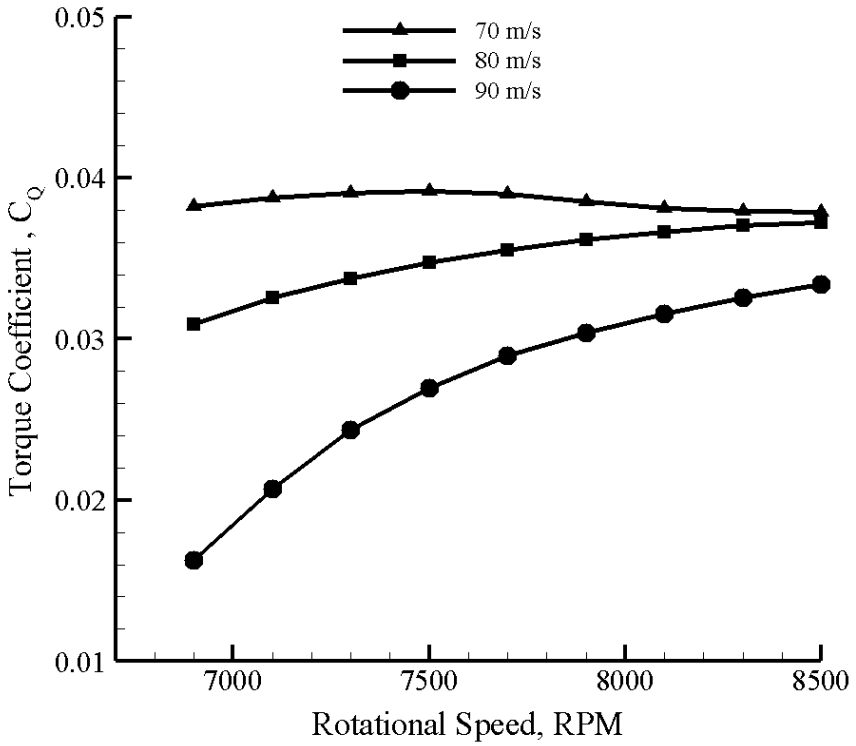

Figure 4.5: Variation of Torque Coefficient with Rotational Speed

The variation in the torque produced by the rotors with respect to the rotational speed at different freestream velocity is shown in figure-4.5. For larger freestream velocities,an increasing trend in the torque with increasing rotational speed was observed. However, the change in the torque was observed to be insignificant for a smaller freestream velocity of 70 m/s. Such differences in torque variation can be explained by the changes in the thrust coefficient as observed in figure-4.4. The aerodynamic torque produced by the rotors is directly proportional to the thrust as shown by equation 3.6. The percentage increase in the propeller thrust for the freestream velocity of 80 m/s and 90 m/s (figure-4.4) was approximately 40% and 85% respectively. This is much higher than the net increase in the thrust for freestream velocity of 70 m/s which was observed to be around 27%. Following this argument, the increase in torque for lower freestream velocities

should be small which is confirmed by figure-4.5.

Furthermore, it can also be observed that the net increase in the torque is not equal to the net increase in thrust because the torque is dependent on other factors such as the correction factor which is shown in equation-3.6. In figure-4.5, it was also observed that the torque required by the propeller at the freestream velocity of 90 m/s was minimum compared to the cases of lower freestream velocity. Propellers require lower power to produce the same thrust at higher induced velocities which is in part with the current observation.

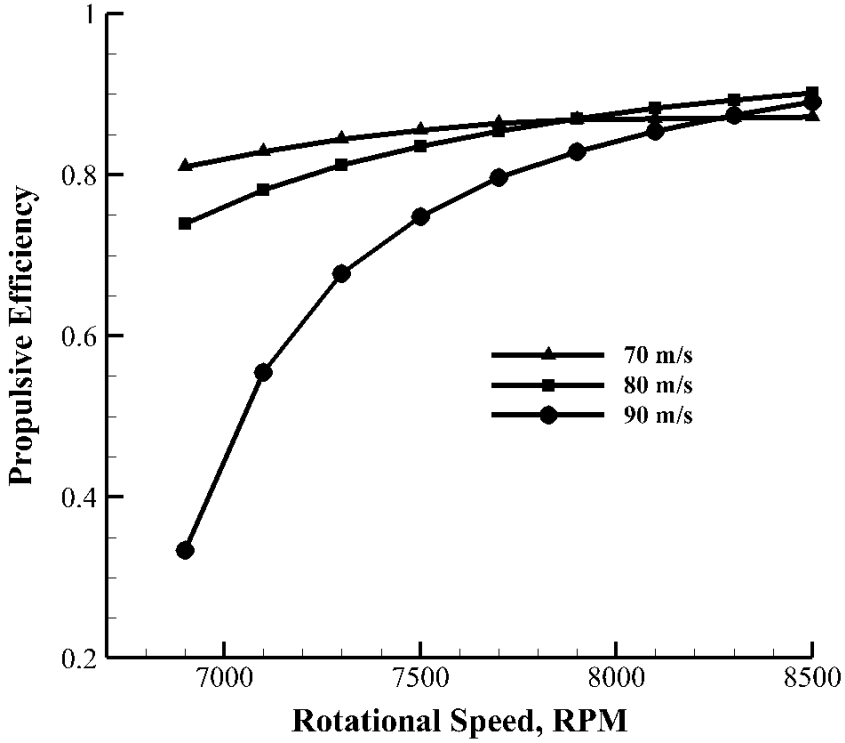

Figure 4.6: Variation of Propulsive Efficiency with Rotational Speed

The variation in the propulsive efficiency with respect to the rotational speed is shown in figure-4.6. The figure shows that for free stream velocity of 70 m/s, propulsive efficiency first increases, reaches to its maximum value of 0.87 at 7897 RPM, and starts to decrease. For other forward speeds, propulsive efficiency increases with rotational speed within our operational bound. For the design point, the propulsive efficiency was found to be 0.835. From the figure, it was also observed that the efficiency of the

propeller was quite low at smaller rotational speeds when the free-stream velocity was set at $90m/s$. The current observation suggests that the propeller should not be operated at lower RPMs when the free-stream velocity is large.

4.3 Effect of Free-stream Velocity

The free-stream velocity of the propeller was varied from 67 m/s to 85 m/s. For three rotational speed 7000 RPM, 7500 RPM, and 8000 RPM, the variation of thrust coefficient, torque coefficient, and propulsive efficiency with respect to the free-stream velocity is studied in this section.

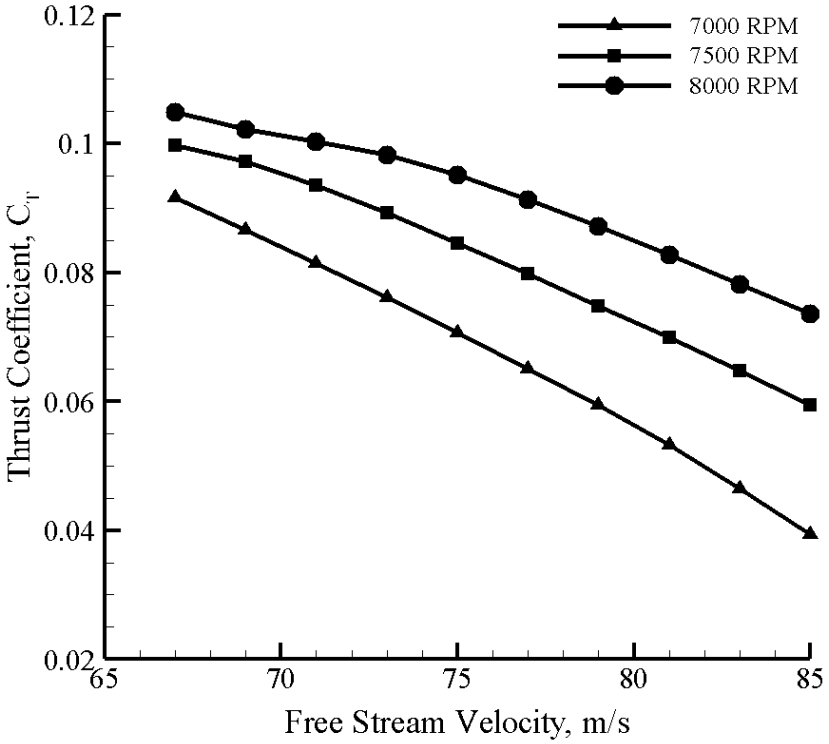

Figure 4.7: Variation of Thrust Coefficient with Free Stream Velocity

Figure-4.7 shows the plot between free-stream velocity and thrust coefficient. The thrust was observed to reduce with increasing free-stream velocity. The thrust was also observed to be the smallest for the lower rotational speed of 7000 RPM. From plot it was observed that the difference between the thrust coefficient for different rotational speed increases with increasing forward speed. At the design point, the thrust coefficient value was found to be 0.0724. The observations currently made are in part with the theory as

explained in the earlier section. The current plot serves as a selection tool for the vehicle design to get an estimate of the propeller performance at different operating conditions.

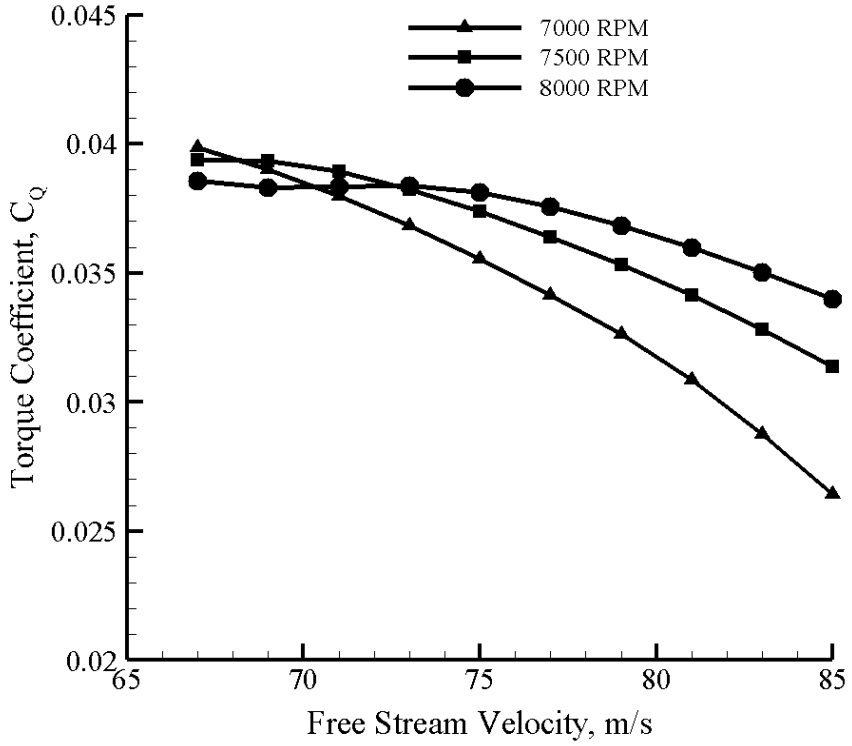

Figure 4.8: Variation of Torque Coefficient with Free Stream Velocity

In figure 4.8 variation of torque coefficient with the freestream velocity was plotted. This shows that the value of the torque coefficient is decreasing with increasing value of free stream velocity for all rotational speeds. The current observation is expected as the thrust is also reducing with increasing free-stream velocity. The aerodynamic torque is directly correlated with the thrust which explains the reduction in the torque coefficient. For the design point, the torque coefficient value was 0.0347.

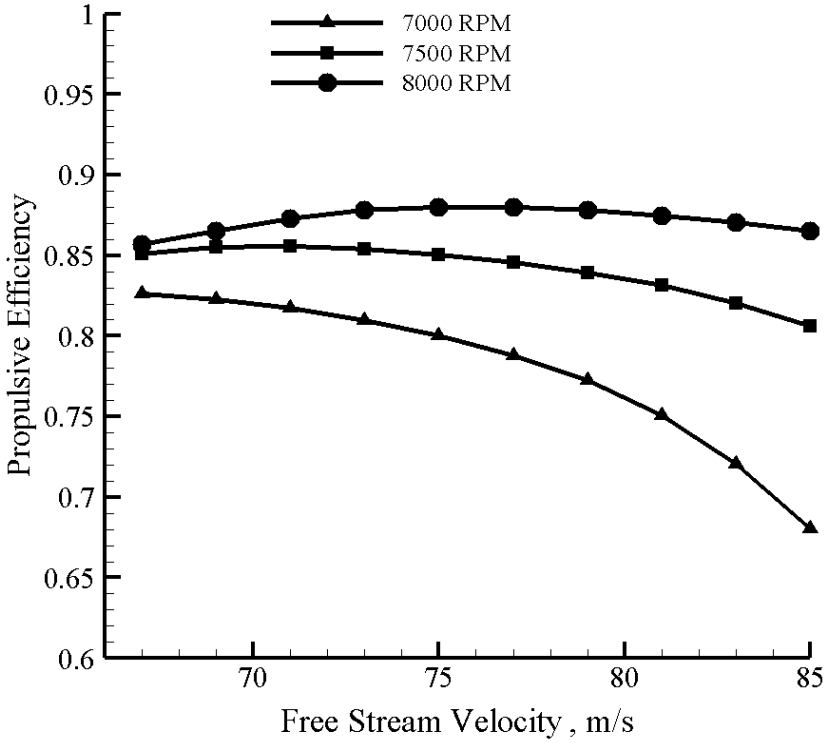

Figure 4.9: Variation of Propulsive Efficiency with Free Stream Velocity

Variation of propulsive efficiency against free stream velocity was plotted in figure-4.9 for different values of rotational speed. The figure shows that for RPM of 8000, the efficiency first increased reached its maximum value, and started to decrease. But for other RPMs, the efficiency was observed to decrease with increasing freestream velocity. The change in the propulsive efficiency with respect to the freestream velocity was observed to be minimum when compared to its change with respect to the rotational speed. At design point the propulsive efficiency was observed to be 0.835. The current phenomena is again in part with the theoretical explanation as presented in the earlier section.

4.4 Effect of Advanced ratio

The plot showing the variation of propeller performance coefficients with respect to the advanced ratio will be discussed in this section. The propeller can have different combination of rotational speed and freestream velocity with same advanced ratio where it shows the same performance. For this, the advanced ratio of the propeller was calculated

using equation-2.1 and variation of thrust coefficient, torque coefficient and propulsive efficiency was observed.

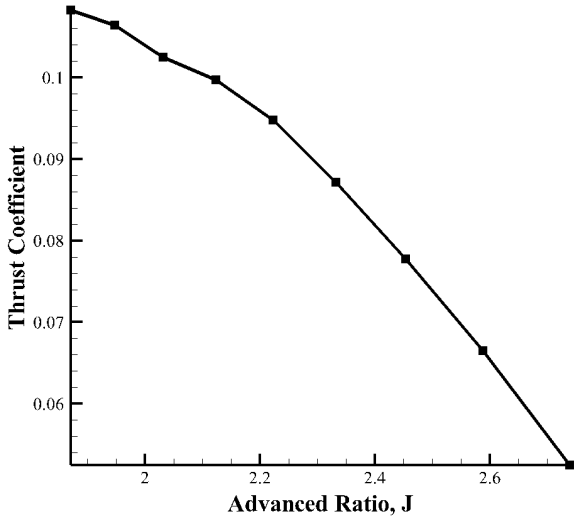

Figure 4.10: Variation of Thrust Coefficient with Advanced Ratio

The graph in figure-4.10 shows the thrust coefficient against the advanced ratio. The trend clearly shows that C_T values decrease when the advanced ratio increases. The advanced ratio can be increased either by increasing freestream velocity or by decreasing rotational speed. This result is similar to the result provided by figure-4.4 and figure-4.7.

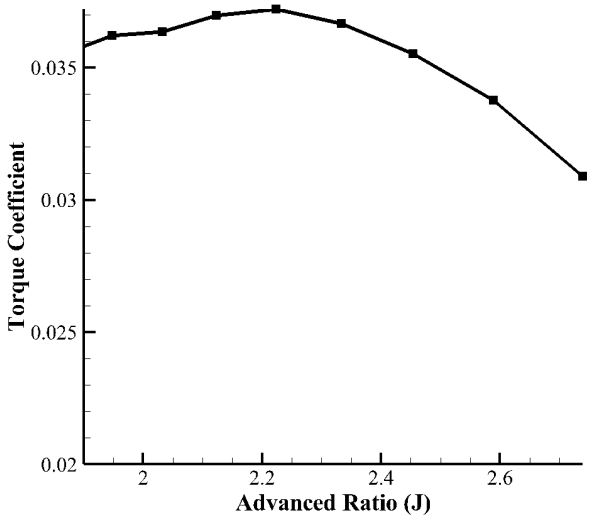

Figure 4.11: Variation of Torque Coefficient with Advanced Ratio

In figure-4.11, the variation of torque coefficient with advanced ratio was plotted. From the figure it can be seen that initially, the variation of torque coefficient is almost constant with increasing value of the advanced ratio. But when the advanced ratio reaches the value of 2.2 it starts to decrease. The trend seen here is similar to the plot shown in McCrink & Gregory (2017) and other literature.

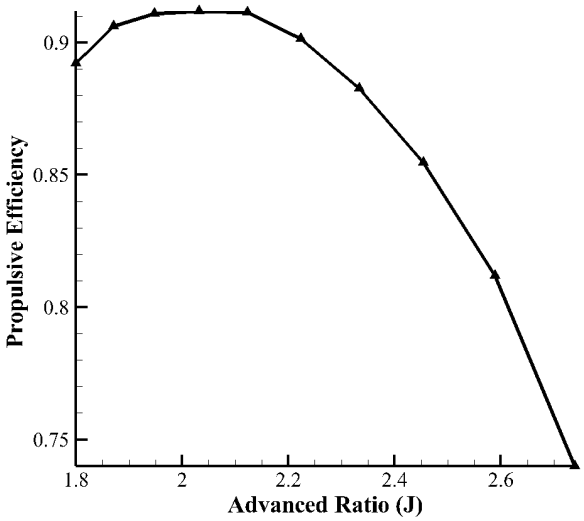

Figure 4.12: Variation of Propulsive Efficiency with Advanced Ratio

The variation of propulsive efficiency against the advanced ratio was plotted in figure-4.12. For the range of advanced ratio obtained from our operational bound, it can be seen that at the beginning propulsive efficiency increased with increasing value of the advanced ratio, reached its maximum value, remained constant for certain a range of advanced ratio, and starts to decrease. In figure-4.3 similar trend can be seen for the experimental data of thin electric APC 11 x 8 propeller extracted from Brandt & Selig (2011).

4.5 One Way FSI Analysis

To perform one way FSI analysis the geometry for fluid domain and blade were created. CFD analysis was performed in ANSYS fluent solver. The pressure load obtained from the CFD was imported to the blade surface in ANSYS static structure setup as shown in figure-4.13. The total deformation and equivalent stress were analyzed.

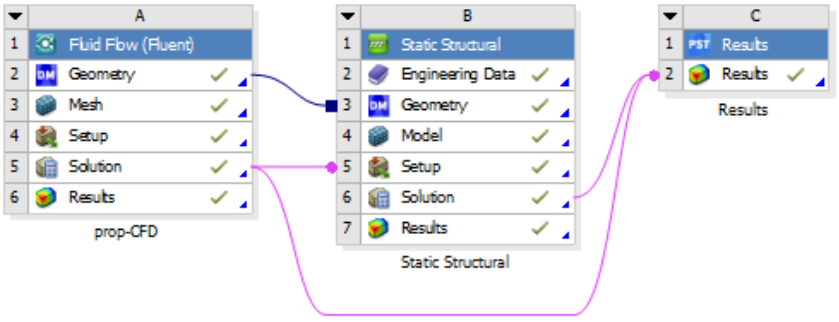

Figure 4.13: Project Schematic for One Way FSI

4.5.1 CFD Analysis

The CFD analysis was performed in ANSYS Fluent to obtained the pressure load, thrust, and torque on the propeller blade. k-ω SST model was selected as the turbulence model due to its suitability for low Reynolds number flow condition with the possibility of flow separation.

4.5.1.1 Boundary Conditions for CFD Analysis

i. Inlet velocity was set to be 80 m/s.

ii. Outlet pressure was assumed to be equivalent to 1 atmospheric pressure at 4000 m.

iii. The rotational velocity of the blade was 7500 RPM.

iv. The surface of the propeller was set as a wall boundary.

4.5.1.2 Computational Domain Details

Fluid domain with generated mesh that was used for CFD analysis is shown in figure-4.14. The mesh generation was done in ANSYS workbench which had about 2 million elements. Flow analysis was performed in ANSYS fluent with residuals set up as $1e^{-}4$.

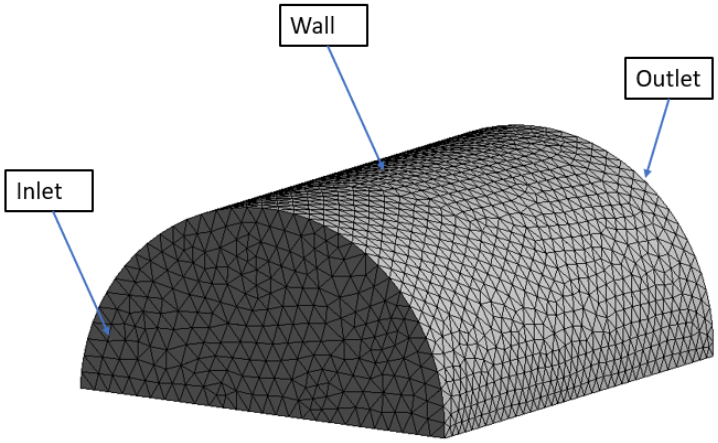

Figure 4.14: Fluid Domain with Generated Mesh

4.5.1.3 Mesh Independence Test

To study the dependency of mesh size on the CFD analysis result, a mesh independence study was carried out. At first, the analysis was performed with a coarse mesh having a 258015 number of elements. The thrust coefficient was found to be 0.04096. The number of elements was increased to 519274 for which the thrust coefficient value increased to 0.05052.

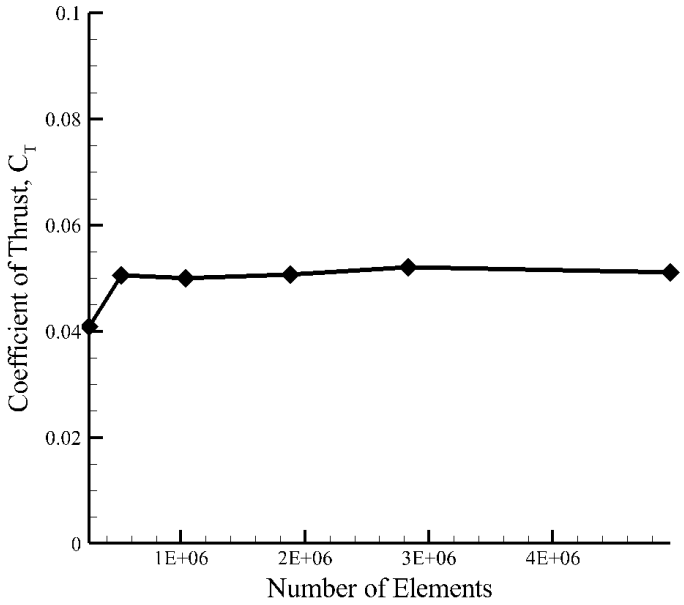

Figure 4.15: Mesh Independence Test

Figure-4.15 shows the variation of thrust coefficient value with the number of elements. Further increase in the elements number after 1883951 has no significant effect on the thrust coefficient value. So all the CFD analyses were performed with the number of elements equal to 1883951.

Plot for pressure contour at a plane 0.1 m away the from axis of rotation is presented in figure-4.16.

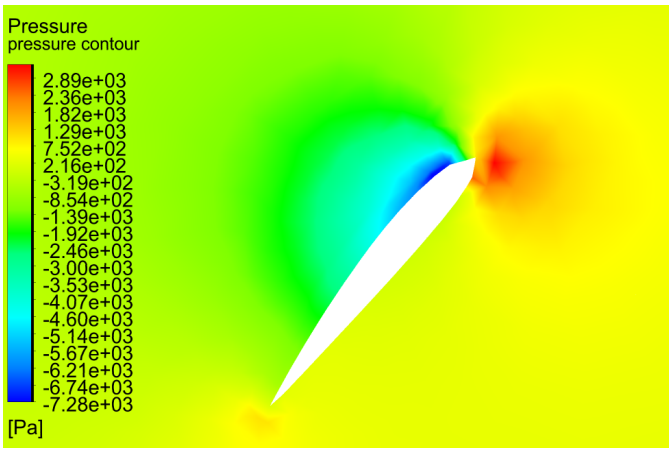

Figure 4.16: Pressure Contour at a Plane 0.1 m from Rotational Axis

The pressure distribution on suction and pressure surfaces of the blade obtained from CFD analysis is shown in figure-4.17.

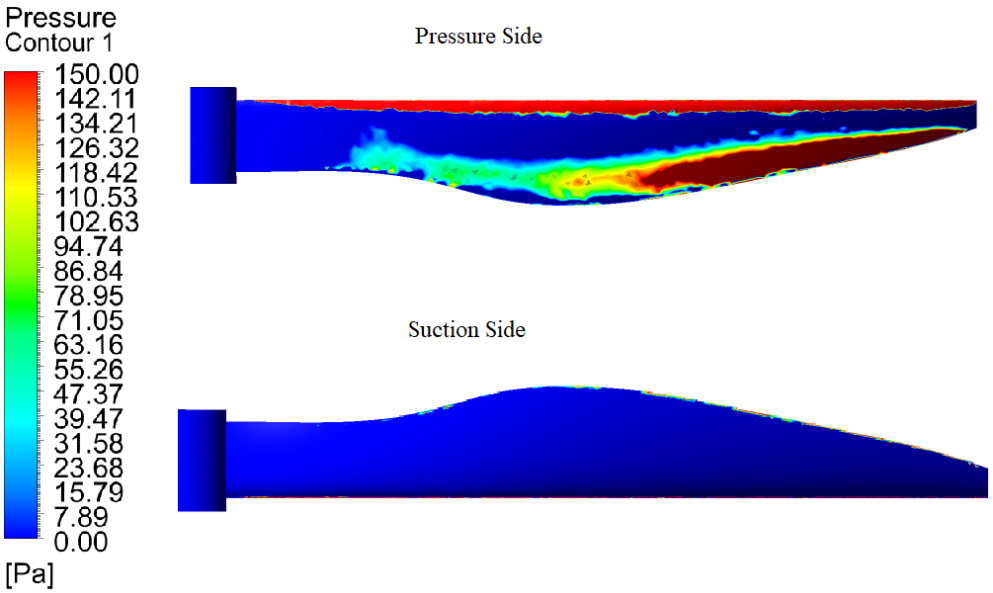

Figure 4.17: Pressure Load Distribution on Blade

4.5.2 Finite Element Analysis

The pressure load obtained from the CFD analysis was imported to the blade surface and FEA analysis was performed in ANSYS static structural workbench to obtain the equivalent stress on blade. For the structural analysis of the blade, structural steel was assigned as blade material. Total stress due to pressure loading was presented in figure-4.18.

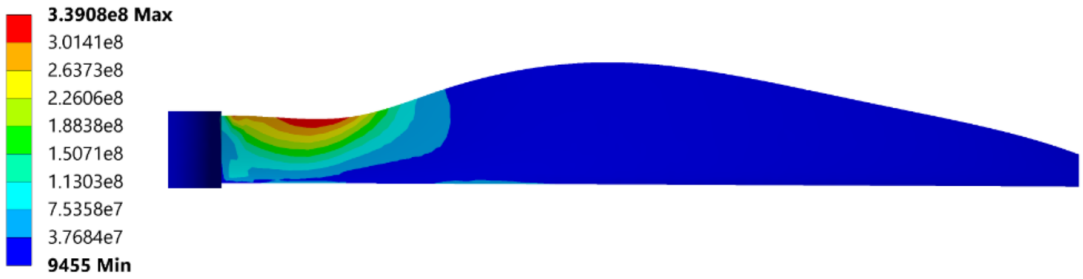

Figure 4.18: Blade Stress Distribution for Baseline Propeller

The maximum stress on the blade was found to be 339.08 Mpa which is higher than the yield point of blade material (250 Mpa). This stress is the result of both pressure and centrifugal loading. Initially, for all sections of baseline propeller's blade, NACA 2412 was chosen as the sectional airfoil. During BEMT analysis the effects of sectional airfoil up to the normalized radial position of 0.3 was neglected. So to reduce the blade stress by increasing root sectional area the NACA 2412 airfoil was replaced by the Clark Y airfoil section. This resulted in an increment of the sectional area by 4.1 mm^2 in the root area.

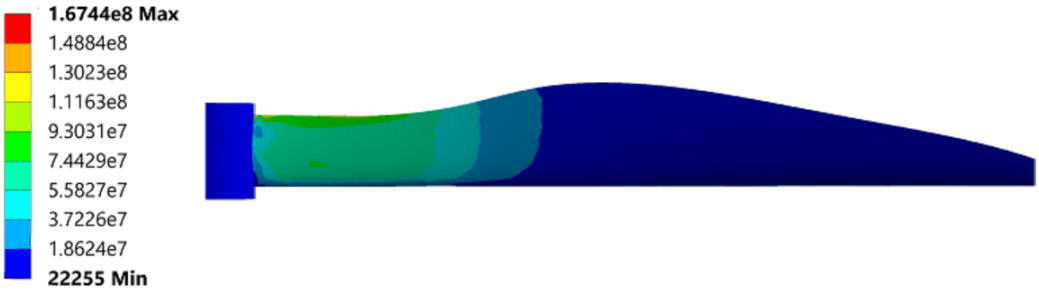

Figure 4.19: Blade Stress Distribution for Modified Geometry

Both CFD and structural analysis was performed for modified blade geometry. The

result shows the total stress decreases significantly. The maximum equivalent stress was found to be 167.44 MPa which is below the yield point.

4.6 Verification of BEMT Prediction with CFD Analysis

The total torque and thrust value obtained from CFD analysis were 2.705 N and 0.38624 N.m respectively. These values were used to calculate the thrust coefficient, torque coefficient, and propulsive efficiency of baseline propeller at its design point. The comparison was made between performance parameters obtained from CFD analysis and BEMT prediction which is presented in table-4.1.

Table 4.1: Verification of BEMT Prediction with CFD Analysis at Design Point

Analysis Method	Thrust Coefficient	Torque Coefficient	Propulsive Efficiency
BEMT Prediction	0.0724	0.0347	83.5%
CFD Analysis	0.05075	0.02852	71.35 %

It was found, for all thrust coefficient, torque coefficient, and propulsive efficiency BEMT prediction is larger than the CFD analysis result.

To compare the BEMT prediction with CFD results at different operating conditions, a number of the simulation were performed by varying free stream velocity. It was found that for all free stream velocity BEMT prediction of thrust coefficient is greater than that of CFD analysis. It was also observed that the variation between BEMT prediction and CFD analysis decreases with increasing value of free stream velocity. The comparison between the result obtained from CFD analysis and BEMT prediction for thrust and torque coefficient is presented in figure-4.20 and figure-4.21 respectively.

For the torque coefficient, BEMT prediction is found to be greater than CFD results for all free stream velocities. Variation on the value of the torque coefficient from two methods is found to be decreased with increasing value of free stream velocity.

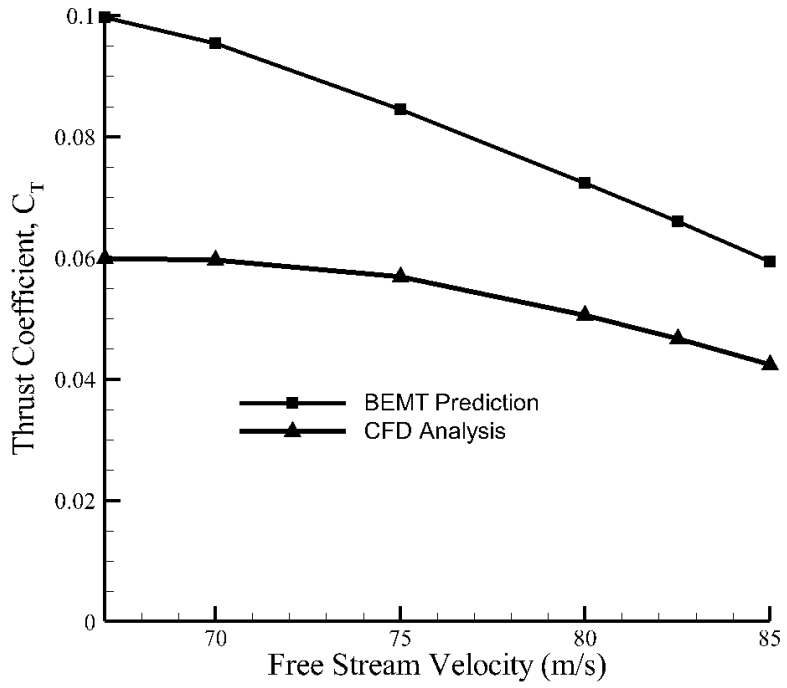

Figure 4.20: Comparison of BEMT Prediction with CFD Results for Thrust Coefficient

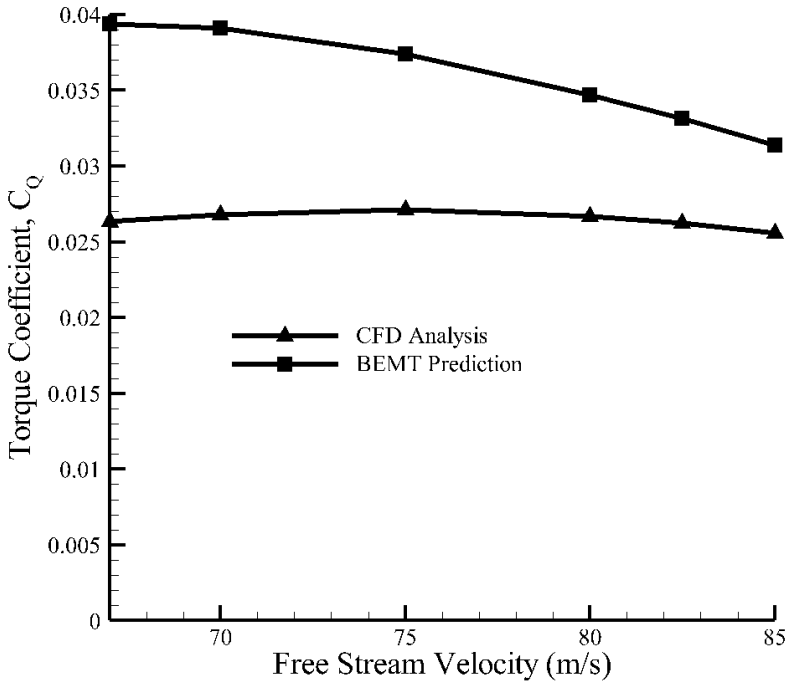

Figure 4.21: Comparison of BEMT Prediction with CFD Results for Torque Coefficient

CHAPTER FIVE: CONCLUSIONS AND RECOMMENDATIONS

5.1 Conclusions

The availability of propeller performance data for the design point and off-design points helps UAVs designer to select the suitable propeller for the specific operating conditions. After validation of the BEMT algorithm and prediction tool, performance analysis of the designed propeller at different operating conditions was carried out. Some of the conclusions that can be made from the current study are listed below:

i. A propeller prediction tool was developed by implementing BEMT in MATLAB programming language.

ii. The validation of the prediction tool was done by comparing the predicted value with experimental data of thin electric APC 11x8 propeller. It was observed that BEMT overestimates the thrust coefficient value for all range of advanced ratio but underestimates the propulsive efficiency value for most of the advanced ratio. But when the advanced ratio is greater than 0.71 BEMT overestimated propulsive efficiency. The trend of thrust coefficient and propulsive efficiency plots were found to be similar to the experimental data.

iii. At the design point, the thrust coefficient, torque coefficient, and propulsive efficiency were found to be 0.0724, 0.0347, and 83.5 % respectively.

iv. The comparison was made between BEMT prediction and CFD analysis at design point for baseline propeller. It was observed that the thrust coefficient, torque coefficient, and propulsive efficiency values obtained from BEMT prediction were higher than those obtained from CFD analysis.

5.2 Recommendations

This research work is limited to the performance prediction of the propeller within a certain operational bound because of the unavailability of post-stall data of airfoil for BEMT algorithm. The aerodynamic database can be extended to the post-stall regions in both directions and performance prediction of the propeller can be done in all possible

operational ranges.

In this research, for stress analysis one way FSI analysis was performed. In future research, two way FSI analysis can be done to get better results on blade stress and deformation.

References

Bhattarai, S., Poudel, K., Bhatta, N., Mahat, S., Bhattarai, S., & Thapa Magar, K. S. (2018). Modeling and development of baseline guidance navigation and control system for medical delivery uav. In *2018 aiaa information systems-aiaa infotech@ aerospace* (p. 0508).

Brandt, J., & Selig, M. (2011). Propeller performance data at low reynolds numbers. In *49th aiaa aerospace sciences meeting including the new horizons forum and aerospace exposition* (p. 1255).

Drela, M. (1989). Xfoil: An analysis and design system for low reynolds number airfoils. In *Low reynolds number aerodynamics* (pp. 1–12). Springer.

Günel, O., Koç, E., & Yavuz, T. (2016). Cfd vs. xfoil of airfoil analysis at low reynolds numbers. In *2016 ieee international conference on renewable energy research and applications (icrera)* (pp. 628–632).

Harrington, R. D. (1951). Full-scale-tunnel investigation of the static-thrust performance of a coaxial helicopter rotor.

Johnson, W. (2013). *Rotorcraft aeromechanics* (Vol. 36). Cambridge University Press.

Liu, X., & He, W. (2017). Performance calculation and design of stratospheric propeller. *IEEE Access*, *5*, 14358–14368.

MacNeill, R., & Verstraete, D. (2017). Blade element momentum theory extended to model low reynolds number propeller performance. *The Aeronautical Journal*, *121*(1240), 835–857.

McCrink, M. H., & Gregory, J. W. (2017). Blade element momentum modeling of low-reynolds electric propulsion systems. *Journal of Aircraft*, 163–176.

Merchant, M., & Miller, L. S. (2006). Propeller performance measurement for low reynolds number uav applications. In *44th aiaa aerospace sciences meeting and exhibit* (p. 1127).

Morgado, J., Vizinho, R., Silvestre, M., & Páscoa, J. (2016). Xfoil vs cfd performance predictions for high lift low reynolds number airfoils. *Aerospace Science and Technology*, *52*, 207–214.

Park, D., Lee, Y., Cho, T., & Kim, C. (2018). Design and performance evaluation of propeller for solar-powered high-altitude long-endurance unmanned aerial vehicle. *International Journal of Aerospace Engineering*, *2018*.

Sissenwine, N., Dubin, M., & Wexler, H. (1962). The us standard atmosphere, 1962. *Journal of Geophysical Research*, *67*(9), 3627–3630.

Traub, L. W., & Cooper, E. (2008). Experimental investigation of pressure measurement and airfoil characteristics at low reynolds numbers. *Journal of aircraft*, *45*(4), 1322–1333.

Wall, D. (2012). *Optimum propeller design for electric uavs* (Unpublished doctoral dissertation).

PUBLICATION

Adhikari,M.,Dura,H.B.,Poudel,L., & Silwal,L.(2020). Theoretical Performance Analysis of Fixed Pitch Propeller Operating at Low Reynolds Number Conditions. Lalitpur, IOE Graduate Conference.

APPENDIX

A: MATLAB Code for BEMT

```
%BLADE ELEMENT MOMENTUM THEORY
% Estimation of local inflow ratio lamda
clc;
clear;
degree = 10;
theta = 2*pi*(degree/360);%Local Pitch Angle
r = 0.1;
Div = 10000;
Inflow = zeros(Div-1,3);
Solidity = 0.027;
F = 1;
Nb = 2;
LCS = 5.7;%Lift Curve Slope
%Radial Position of section with respect to Propeller Radius;
TSR = 0;
lamdar = sqrt(((Solidity*LCS)/(16*F)-(TSR*0.5))^2 + (Solidity*LCS*r*theta)/(8*
F)) -
((Solidity*LCS)/(16*F) - (TSR*0.5));
for j = 1:Div-1
r = j/Div;
fori = 1 : 6
lamda_prev = lamdar;
phi = lamdar/r;
f = 0.5*Nb*((1-r)/(r*phi));
F = (2/pi)*acos(exp(-f));
lamdar = sqrt(((Solidity*LCS)/(16*F) - (TSR*0.5))^2 + (Solidity*LCS*r*
theta)/(8*F)) - ((Solidity*LCS)/(16*F) - (TSR*0.5));
Error = lamdar - lamda_prev;
ifError == 0
```

```
break
end
end
Inflow(j,1) = 1/Div * j;
Inflow(j,2) = lamdar;
Inflow(j,3) = F;
end
%CalcuationofTorqueCoefficeintandPowerCoefficient%NumericalIntegrationbyusingTra
0.011;
CTi = 0;
CPi = 0;
CPP = Solidity * cd0 * 0.125;
fork = 1 : Div - 2
a = k/Div;
b = (k + 1)/Div;
lamdar = (Inflow(k,2) + Inflow(k + 1,2))/2;
CT = CTi + Inflow(k,3) * 4 * lamdar^2 * (b - a) * (a + b) * 0.5;
CTi = CT;
CP = CPi + 4 * Inflow(k,3) * lamdar^3 * (b - a) * (a + b) * 0.5;
CPi = CP;
end
CP = CPP + CP;
```

B: MATLAB code to create aerodynamics Database with XFOIL

```
% Airfoil_Performance_Database
clear;
clc;
%Inputs for XFOIL input file
NACA =' 4412';
RN =' 6000000';
xfoil_output file =' Xfoil_output.txt';


if (exist(xfoil_output file,' file'))
delete(xfoil_output file);
end
createInput(NACA, RN, xfoil_output file)
cmd = 'xfoil.exe < xfoil_input file.txt';
status,result
= system(cmd);


fid = fopen(xfoil_output file,' rt');
if fid == −1
fprintf("Error!!Check File Name");
else
for i = 1 : 12
fgetl(fid);
end
polar = fscanf(fid,' polar = polar';
polar = polar(:, 1 : 3);
end
fclose(fid);


[clmax, Rowmax] = max(polar(:,2));
clmin, Rowmin
= min(polar(:,2));
AOA = polar(:,1);
cl = polar(:,2);
```

```
cd = polar(:,3);
figure(1);
plot(AOA,cl);
grid on;
xlabel("Angle of Attack, AoA");
ylabel("Coefficient of Lift, Cl");
title("AOA vs Cl");
figure(2)
plot(AOA,cd);
grid on;
xlabel("Angle of Attack, AoA");
ylabel("Coefficient of Drag, Cd");
title("AOA vs Cd");
lift_curve_slope = (polar(Rowmax-20,2)-polar(Rowmin+60,2))/(polar(Rowmax-
20,1) - polar(Rowmin + 60,1));
fprintf('The lift curve slope is %g', lift_curve_slope);
```

C: MATLAB code to generate coordinates of propeller for 3d modeling of base-line propeller

```
clc;
clear;
%Operating Conditions and Geometry of Propeller
Meu = 0.00001661;Rho = 0.8198;Div = 10; Dia = (10*25.4)/1000;V = 80; W = 7500;
prop_geometry = zeros(Div,7);
for i = 1:Div
prop_geometry(:,1) = (1/Div:1/Div:1);
prop_geometry(i,2) = (W*2*pi()/60)*prop_geometry(i,1)*(Dia*0.5); prop_geometry(i,3)
= atan(V/prop_geometry(i,2))*360/(2*pi); prop_geometry(i,4) = (0.084241-0.85789*(i/Div)
+4.7176*(i/Div)^2 – 9.6225 * ...(i/Div)^3 + 8.5004 * (i/Div)^4 – 2.7959 * (i/Div)^5) * Dia *
1000;
prop_geometry(i,5) = 8;
prop_geometry(i,6) = prop_geometry(i,3) + prop_geometry(i,5);
prop_geometry(i,7) = (Rho * sqrt(V^2 + (prop_geometry(i,2))^2)...
* prop_geometry(i,4))/Meu;
endblade_coordinates = zeros(35,3,Div);
for j = 1 : Div
unit_coordinate = xlsread('NACA_2412_Co_ordinates');
scaled_coordinates = prop_geometry(j,4)* unit_coordinate;
scaled_coordinates(:,3) = prop_geometry(j,1)*(0.5*Dia)*1000;
blade_coordinates(:,:,j) = scaled_coordinates;
blade_angle = prop_geometry(j,6);

A = cosd(blade_angle);
B = sind(blade_angle);
rotated_coordinates = scaled_coordinates;
rotated_coordinates(:,1) = scaled_coordinates(:,1)*A+B*scaled_coordinates(:,2);
rotated_coordinates(:,2) = scaled_coordinates(:,1)*(-B)+A*scaled_coordinates(:,2);
blade_coordinates(:,:,j) = rotated_coordinates;
```

```
plot3(blade_coordinates(:,1,j),blade_coordinates(:,2,j)...
,blade_coordinates(:,3,j))
hold on;
end

for x = 1:Div
filename = 'Propeller_Coordinates.xlsx';
sheet = x;
xlRange = 'A1';
xlswrite(filename,blade_coordinates(:,:,x),sheet,xlRange);
end
```

D: Airfoil Data for NACA 2412

1.000000	0.001300	0.600000	-0.027600
0.950000	0.011400	0.700000	-0.021400
0.900000	0.020800	0.800000	-0.015000
0.800000	0.037500	0.900000	-0.008200
0.700000	0.051800	0.950000	-0.004800
0.600000	0.063600	1.000000	-0.001300
0.500000	0.072400		
0.400000	0.078000		
0.300000	0.078800		
0.250000	0.076700		
0.200000	0.072600		
0.150000	0.066100		
0.100000	0.056300		
0.075000	0.049600		
0.050000	0.041300		
0.025000	0.029900		
0.012500	0.021500		
0.000000	0.000000		
0.012500	-0.016500		
0.025000	-0.022700		
0.050000	-0.030100		
0.075000	-0.034600		
0.100000	-0.037500		
0.150000	-0.041000		
0.200000	-0.042300		
0.250000	-0.042200		
0.300000	-0.041200		
0.400000	-0.038000		
0.500000	-0.033400		